International Journal for Multidisciplinary Research (IJFMR)
E-ISSN: 2582-2160 ● Website: www.ijfmr.com ● Email: editor@ijfmr.com

Thermo-Mechanical Analysis of Zirconia-ZIF-8 Reinforced Polyimide Composite Coatings by Numerical and Finite Element Methods

Avilash Maji[1], Siddhant Gokhale[2]

[1,2]Final Year B.Tech Student, Department of Mechanical Engineering, National Institute of Advanced Manufacturing Technology, Ranchi, India

Abstract:
The thermo–mechanical behaviour of a Zirconia-Polyimide-ZIF-8 composite coating is examined in this study, with a specific focus on electric vehicle battery thermal management applications. Effective thermo-mechanical properties were derived using the Maxwell–Eucken model and the Rule of Mixtures for a 1:1:1 weight fraction blend. A cuboidal coating geometry of 100 mm × 100 mm × 10 mm was subjected to a hot surface temperature of 300°C and a convective cold boundary at 20°C with a forced convection coefficient of 20 W/m²·K. Steady-state coupled thermal and structural analyses were conducted in ANSYS Workbench 2026 R1. The composite produced a lower cold-surface temperature and reduced thermal stress relative to monolithic zirconia, while exhibiting greater deformation and strain - collectively reflecting improved thermal insulation alongside enhanced stress relaxation capability.

Keywords: Thermal Barrier Coating, Maxwell-Eucken Modelling, Rule of Mixtures, ZIF-8, Polyimide, Finite Element Analysis

1. Introduction

The rapid growth of electric vehicles, aerospace systems and advanced thermal engineering platforms has substantially increased the demand for versatile thermal barrier coatings. Such coatings serve a dual function: shielding structural components from cyclic thermal exposure while enhancing overall thermal efficiency. Among conventional thermal barrier coating materials, Zirconia (Yttria Stabilized Zirconia) is the most widely adopted on account of its low thermal conductivity, high melting temperature and excellent chemical stability [1]. Within EV battery architectures, thermally insulating layers have been extensively studied to mitigate thermal runaway risks and sustain uniform temperature distributions during operation. Despite these merits, traditional ceramic coatings are constrained by inherent brittleness, elevated thermal stress accumulation and susceptibility to cracking under restricted thermal expansion conditions.

A fundamental limitation of conventional thermal barrier coatings is the conflict between thermal insulation and mechanical performance. Materials that offer high thermal resistance tend to exhibit elevated stiffness combined with low strain tolerance, which promotes stress concentration and accelerates premature failure under cyclic thermal loading. Overcoming these limitations requires advanced composite coating systems capable of simultaneously delivering superior insulation and improved thermo–mechanical stability.

In this context, hybrid composite materials that integrate ceramic, polymeric and porous framework constituents present a compelling design strategy. The present study proposes a novel composite coating formulated from Zirconia, Polyimide and ZIF-8 in equal weight fractions. Within this system, Zirconia contributes thermo–mechanical stability, Polyimide imparts flexibility and ZIF-8 delivers ultra-low thermal conductivity through its inherently porous architecture. Effective composite properties are first established through analytical homogenisation, and thermo–mechanical performance is subsequently evaluated under boundary conditions representative of EV battery environments.

By coupling analytical modelling with finite element simulations in ANSYS Workbench, this research aims to address the limitations of traditional thermal barrier coatings through improved thermal insulation and reduced stress generation, thereby enhancing coating reliability for modern thermal management applications.

2. Literature Review

The increasing demand for high-performance thermal barrier coatings in thermal and energy systems has driven significant evolution in coating morphology and composition. Zirconia-based coatings are the most widely investigated thermal barrier systems owing to their low thermal conductivity, phase stability and elevated temperature resistance [1]. Contemporary developments have focused on enhancing durability through doped, nanostructured, multilayered and gradient architectures aimed at overcoming thermal stress accumulation and degradation under cyclic loading. These advances collectively underscore the need for more resilient material systems beyond monolithic ceramics.

Polymer-based coatings have been explored as alternatives or complements to ceramic layers. Polymer matrix systems offer improved flexibility and low thermal conductivity, enabling coatings with enhanced strain tolerance relative to brittle ceramics [2]. Ceramic–polymer hybrid configurations have demonstrated favourable results by combining ceramic insulation performance with polymeric mechanical compliance, thereby reducing crack propagation and improving adhesion [3].

Metal–organic frameworks, and ZIF-8 in particular, have recently emerged as thermal insulation candidates due to their highly porous structure and low bulk density. Studies combining ZIF-8 with Zirconia have reported enhanced thermal functionality and multifunctional performance, pointing to applications extending well beyond the biomedical domain into thermal barrier systems [4]. ZIF-8-based composites with inorganic matrices have further demonstrated notable thermal loading behaviour relevant to such hybrid systems [17]. Collectively, these investigations motivate the development of advanced hybrid composite coatings that simultaneously address the thermal and mechanical deficiencies of traditional thermal barrier coatings, as pursued in the present work.

3. Methodology

3.1 Selection of Materials

3.1.1 Zirconia

Yttria Stabilized Zirconia (YSZ) was selected as the primary ceramic constituent on account of its well-established application as a thermal barrier coating material, particularly its high melting point [5]. It further exhibits low thermal conductivity and excellent resistance to oxidation at elevated temperatures. The properties adopted in this study are: density 6000 kg/m³, thermal conductivity 2 W/m·K, coefficient of thermal expansion 9.6×10^{-6} °C^{-1}, Young's modulus 205 GPa and Poisson's ratio 0.31 [6, 17]. These

values collectively provide the structural rigidity and thermal resistance required for high-temperature coating applications.

3.1.2 Polyimide

Polyimide was incorporated to introduce mechanical compliance and supplementary thermal insulation within the composite. Unlike brittle ceramics, polyimide exhibits high flexibility, good thermal resistance and low thermal conductivity, making it well-suited for stress relaxation under thermal gradients. Its key properties are: density 1420 kg/m³, elastic modulus 2.5 GPa, coefficient of thermal expansion 30×10^{-6} °C^{-1} [7], thermal conductivity 0.12 W/m·K, specific heat 1900 J/kg·K and Poisson's ratio 0.34. A glass transition temperature of approximately 300°C [8] defines the upper operational thermal limit considered in this study.

3.1.3 Zeolitic Imidazolate Framework-8 (ZIF-8)

ZIF-8 was selected due to its porous metal–organic framework architecture, which confers extremely low thermal conductivity and lightweight characteristics [9, 10]. The intrinsic porosity of the framework restricts heat transfer pathways, thereby enhancing thermal insulation. Its loading and thermal behaviour within inorganic composite matrices has also been recently characterised [17]. The properties adopted are: density 950 kg/m³ [11], thermal conductivity 0.165 W/m·K [10], coefficient of thermal expansion 10.5×10^{-6} °C^{-1}, Young's modulus 5.6 GPa and Poisson's ratio 0.4 [12].

3.2 Assumptions

3.2.1 For Equivalent Property Calculation

- Materials are assumed to be isotropic and homogeneous.
- Perfect bonding is assumed to exist among all constituent phases.
- No interfacial thermal resistance is considered.
- An equal weight fraction (1:1:1) distribution is assumed to be uniformly dispersed throughout the composite.
- Material properties are assumed to be temperature-independent within the operating range.

3.2.2 For Cold Wall Temperature Calculation

- One-dimensional steady-state heat conduction is assumed.
- Heat transfer occurs exclusively along the thickness direction.
- Side faces are treated as perfectly insulated (adiabatic).
- A constant convection coefficient for ambient air is assumed.
- Radiation heat transfer effects are neglected.

3.3 Equivalent Property Calculation

3.3.1 Thermal Conductivity – Maxwell-Eucken Model

The effective thermal conductivity of the composite was computed using the Maxwell–Eucken formulation extended to multiphase systems [18]:

$$k_{eff} = k_m \times \frac{[\, k_f + 2k_m + 2\,\varphi(k_f - k_m)\,]}{[\, k_f + 2k_m - \varphi(k_f - k_m)\,]} \qquad (1)$$

where k_{eff} is the effective thermal conductivity, k_m is the matrix thermal conductivity, k_f is the filler thermal conductivity and φ is the volume fraction. The model captures the effect of dispersed insulating phases within a continuous medium. The filler conductivity k^f is evaluated using the Rule of Mixtures.

3.3.2 Rule of Mixtures

Density, coefficient of thermal expansion, Young's modulus and Poisson's ratio were each determined through weighted averaging of constituent properties [13]:

$$P_{eff} = \sum V_i P_i \quad (2)$$

where P_{eff} is the effective property, V_i is the weight fraction and P_i is the corresponding property of constituent i.

3.4 Calculation of Cold Wall Temperature

A cuboidal coating block of 100 mm × 100 mm × 10 mm was adopted for the analytical heat transfer evaluation. The hot surface temperature was fixed at 300°C, a value coinciding with the glass transition temperature of Polyimide and therefore representing the safe operational thermal limit of the composite. The opposing cold surface was exposed to ambient air at 20°C with a forced convection coefficient of 20 W/m²·K, representative of moderate airflow conditions in EV battery environments.

Applying heat flux continuity at the cold surface under steady-state one-dimensional conditions yields [14]:

$$k\left(\frac{T_h - T_c}{l}\right) = h(T_c - T_\infty) \quad (3)$$

where k is thermal conductivity, L is coating thickness (0.01 m), h is the convective heat transfer coefficient, T_h is the hot wall temperature, T_c is the cold wall temperature and T_∞ is the ambient temperature. This relation was applied independently to the composite and to monolithic YSZ using their respective conductivity values.

3.5 ANSYS Workbench Setup

Figure 1 (a-b): Model and Meshing

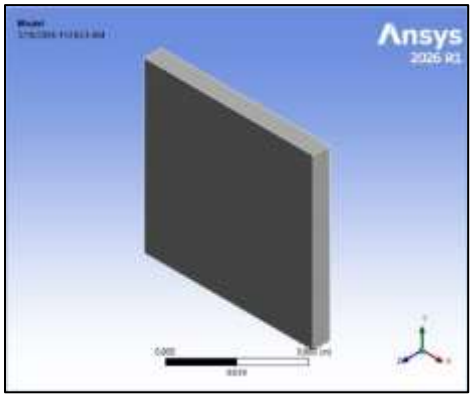

(a) ANSYS Workbench Model for Analysis

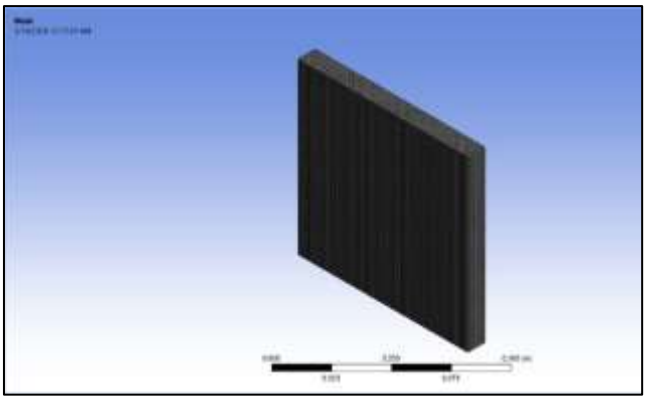

(b) ANSYS Workbench Meshing

Table 1: Meshing Parameters

Meshing Parameter	**Value**
Physics Preference	Mechanical
Element Type Generation	Programme-controlled tetrahedral elements
Element Order	Program Controlled
Element Size	1.0×10^{-3} m (1 mm)
Mesh Sizing	Adaptive
Transition	Fast

Span Angle Center	Coarse
Smoothing	Medium
Mesh Defeaturing	Yes (Defeature Size: 3.5333×10^{-5} m)
Total Number of Nodes	436,421
Total Number of Elements	100,000

3.5.1 Steady-State Thermal Analysis

- Geometry: three-dimensional cuboid (100 × 100 × 10 mm).
- Hot surface: fixed temperature boundary condition at 300°C.
- Cold surface: convective boundary condition with ambient air ($h = 20$ W/m²·K, $T_\infty = 20$°C).
- Remaining faces: treated as adiabatic.
- Uniform initial temperature applied throughout the domain.
- Mesh generated using programme-controlled tetrahedral elements.

3.5.2 Thermo-Structural Coupling

The temperature distribution from the steady-state thermal analysis was imported into a Static Structural module as the driving thermal body load [15, 16].

3.5.3 Boundary Conditions for Structural Analysis

- The hot surface was constrained with a fixed support to represent a worst-case scenario in which thermal expansion is fully restricted.
- Thermal loads were applied as a distributed body temperature field transferred directly from the thermal solution.

This coupled modelling approach enables thermo–mechanical evaluation under realistic constrained thermal loading without the introduction of experimental parameters.

4. Results And Discussion

4.1 Equivalent Property Estimation

Application of the Maxwell–Eucken model [18] and Rule of Mixtures to the three-constituent system produced the effective thermo–mechanical properties listed in Table 1. The most notable outcome is a marked reduction in effective thermal conductivity relative to monolithic zirconia, attributed to the presence of low-conductivity polyimide and the highly porous ZIF-8. The composite density is also substantially lower than that of YSZ, reflecting the lightweight character of the polymeric and framework phases.

Table 2: Effective Thermo-Mechanical Properties of the Zirconia–Polyimide–ZIF-8 Composite

Property	Value
Density (kg/m³)	2787.21
Thermal Conductivity (W/m·K)	0.45
Coefficient of Thermal Expansion ($\times 10^{-6}$ /K)	16.68
Specific Heat (J/kg·K)	1177.23
Young's Modulus (GPa)	70.96
Poisson's Ratio	0.35

The coefficient of thermal expansion is elevated relative to pure zirconia, primarily due to the influence of polyimide's high expansion behaviour. The equivalent Young's modulus is reduced compared to

zirconia, reflecting enhanced compliance of the hybrid system. The Poisson's ratio exhibits a moderate value indicative of balanced elastic behaviour. Collectively, the effective properties mark a transition from a stiff ceramic material to a thermally insulating and mechanically compliant hybrid composite well-suited to thermal barrier applications.

4.2 Cold Wall Temperature Comparison

Cold wall temperature calculations were performed under identical thermal boundary conditions for both the composite and monolithic YSZ. As shown in Table 2, the composite attained a cold surface temperature of 213.85°C compared to 274.55°C for YSZ - a reduction of approximately 60.7°C.

Table 3: Cold Wall Temperature Comparison

Material	Cold Wall Temperature (°C)
Composite (Zirconia–Polyimide–ZIF-8)	213.85
Yttria Stabilized Zirconia (YSZ)	274.55

This reduction is a direct consequence of the composite's lower effective thermal conductivity, which restricts heat flux across the coating thickness. Consequently, less thermal energy reaches the cold surface, improving overall insulation performance. From an application standpoint, this lower cold wall temperature is particularly advantageous for EV battery coatings where minimising heat transfer to adjacent sensitive components is a primary design requirement.

4.3 Finite Element Analysis Comparison

4.3.1 Temperature Profile Comparison

Figure 2 (a-b): Thermal Profiles

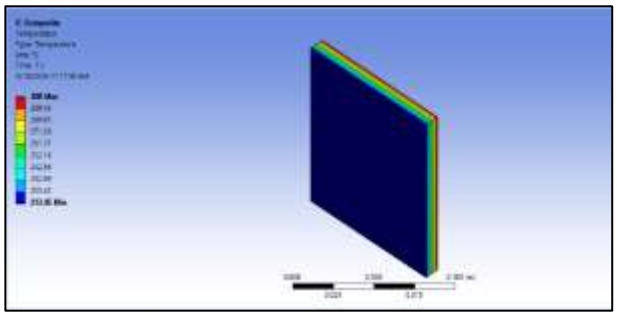

(a) ANSYS Workbench Temperature Profile for Composite

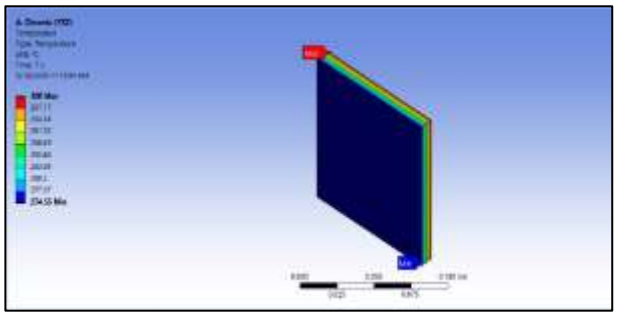

(b) ANSYS Workbench Temperature Profile for Zirconia

Steady-state thermal simulations produced a steeper and more pronounced temperature gradient across the composite thickness relative to YSZ. The composite's greater thermal resistance resulted in stronger temperature attenuation between the hot and cold surfaces. YSZ, possessing comparatively higher thermal conductivity, permitted more uniform heat penetration through the coating cross-section.

4.3.2 Total Deformation Comparison

Figure 3 (a-b): Deformation Profiles

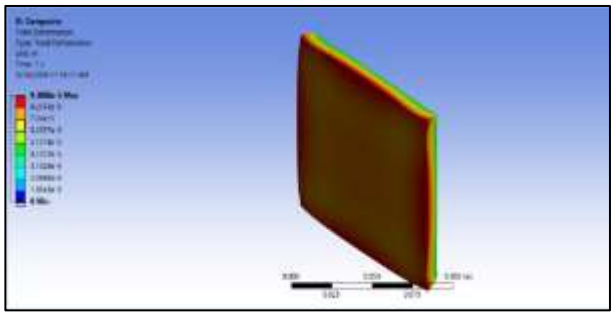

(a) ANSYS Workbench Total Deformation Profile for Composite

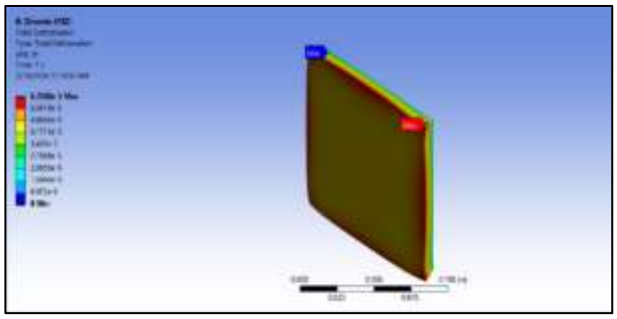

(b) ANSYS Workbench Total Deformation Profile for Zirconia

Structural analysis indicated greater total deformation in the composite block. The reduced stiffness combined with a higher effective thermal expansion coefficient enabled more pronounced dimensional change under the applied thermal load. This elevated deformation is better understood as enhanced flexibility rather than structural weakness, as it reflects the material's capacity to accommodate thermal expansion rather than rigidly resist it.

4.3.3 Equivalent (Von Mises) Stress Comparison

Figure 4 (a-b): Stress Profiles

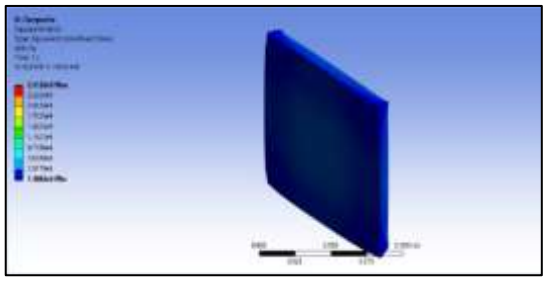

(a) ANSYS Workbench Equivalent Stress Profile for Composite

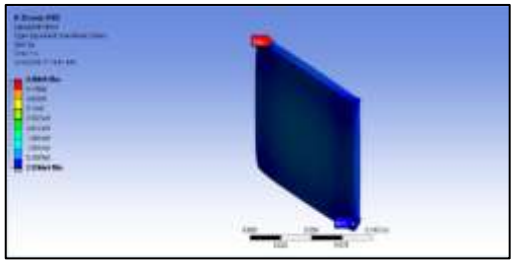

(b) ANSYS Workbench Equivalent Stress Profile for Zirconia

The von Mises stress developed within the composite was lower than that in YSZ under identical constraint conditions. The reduced elastic modulus of the composite facilitated stress redistribution, mitigating the stress concentrations arising from fully restrained thermal expansion. This behaviour is indicative of improved resistance against thermally induced cracking.

4.3.4 Thermal Strain Comparison

Figure 5 (a-b): Thermal Strain Profiles Analysis

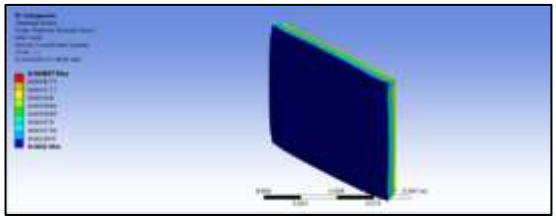

(a) ANSYS Workbench Thermal Strain Profile for Composite

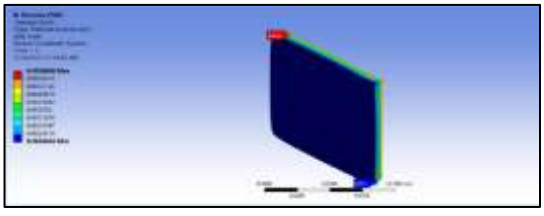

(b) ANSYS Workbench Thermal Strain Profile for Zirconia

Thermal strain values were higher in the composite, consistent with its larger effective coefficient of thermal expansion. Crucially, this elevated strain developed alongside reduced stress magnitudes - a pairing that is indicative of effective strain accommodation. The coexistence of higher strain and lower stress demonstrates thermo–mechanical compatibility well-suited to constrained heating environments.
Viewed collectively, the finite element results confirm that while YSZ provides greater rigidity, the proposed composite achieves superior thermal insulation and more effective stress mitigation, making it a more suitable candidate for advanced thermal barrier coating applications.

5. Conclusion

This study established the thermo–mechanical feasibility of a Zirconia-Polyimide-ZIF-8 composite as an advanced thermal barrier coating through combined analytical modelling and finite element simulation. The composite delivered improved thermal insulation and reduced thermal stress relative to conventional YSZ, while accommodating greater strain owing to its enhanced mechanical compliance. These characteristics indicate strong potential for thermal management applications, particularly EV battery protection. Future work may focus on optimising constituent weight fractions to achieve a balanced insulation–stability profile, exploring alternative constituent materials for further performance improvement, and developing fabrication methodologies to validate the proposed composite through experimental investigation and practical implementation.

References

1. A.H. Esmaeilkhanian, F. Sharifianjazi, E. Ahmadi, A. Ijadi, H. Meskher, R. Zarei, M. Nili-Ahmadabadi, M. Irandoost, N. Karimi, “Thermal barrier coating with improved durability: An overview of doped, nanostructured, multilayered, and gradient-structured zirconia-based thermal barrier coatings,” Materials Today Communications, 2023, 37, 107514. https://doi.org/10.1016/j.mtcomm.2023.107514
2. [2 of thermal barrier coatings onto polyimide matrix composites via air plasma spray process,” Surface and Coatings Technology, 2012, 207, 421–429. https://doi.org/10.1016/j.surfcoat.2012.07.042
3. P. Luangtriratana, B.K. Kandola, P. Myler, “Ceramic particulate thermal barrier surface coatings for glass fibre-reinforced epoxy composites,” Materials & Design, 2014, 68, 232–244. https://doi.org/10.1016/j.matdes.2014.11.057
4. L. Su, Q. Wu, L. Tan, H. Ziao, C. Fu, X. Ren, N. Xia, Z. Chen, X. Ma, X. Lan, Q. Zhang, X. Meng, “High biocompatible ZIF-8 coated by ZrO_2 for chemo-microwave thermal tumor synergistic therapy,” ACS Applied Materials & Interfaces, 2019, 11 (11), 10520–10531. https://doi.org/10.1021/acsami.8b22177
5. W.D. Callister, Jr., D.G. Rethwisch, Materials Science and Engineering: An Introduction, John Wiley & Sons, Inc., 2018.
6. Polyimide. https://www.mit.edu/~6.777/matprops/polyimide.htm
7. S. Numata, S. Oohara, J. Imaizumi, N. Kinjo, “Thermal expansion behavior of various aromatic polyimides,” Polymer Journal, 1985, 17 (8), 981–983.
8. M. Khalil, S. Saeed, Z. Ahmad, “Properties of binary polyimide blends containing hexafluoroisopropylidene group,” Journal of Macromolecular Science Part A, 2006, 44 (1), 55–63. https://doi.org/10.1080/10601320601044476

9. E. Lasseuguette, L. Fielder-Dunton, Q. Jian, M. Ferrari, "The effect of solution casting temperature and ultrasound treatment on PEBAX MH-1657/ZIF-8 mixed matrix membranes morphology and performance," Membranes, 2022, 12 (6), 584. https://doi.org/10.3390/membranes12060584
10. X. Zhang, J. Jiang, "Thermal conductivity of zeolitic imidazolate framework-8: A molecular simulation study," The Journal of Physical Chemistry C, 2013, 117 (36), 18441–18447. https://doi.org/10.1021/jp405156y
11. S. Liu, L. Sun, Y. Zhou, L. Liu, "Heat capacities and thermodynamic properties of a Zn-based zeolitic imidazolate framework," Journal of Thermal Analysis and Calorimetry, 2018, 135 (6), 3191–3196. https://doi.org/10.1007/s10973-018-7605-0
12. M. Erkartal, M. Durandurdu, "Pressure-induced amorphization, mechanical and electronic properties of zeolitic imidazolate framework (ZIF-8)," Materials Chemistry and Physics, 2019, 240, 122222. https://doi.org/10.1016/j.matchemphys.2019.122222
13. H.M.A. Abdalla, "Review of rules of mixture for effective elastic properties in fibrous and particulate composite materials," Composite Structures, 2025, 367, 119216. https://doi.org/10.1016/j.compstruct.2025.119216
14. F.P. Incropera, D.P. DeWitt, T.L. Bergman, A.S. Lavine, Fundamentals of Heat and Mass Transfer, John Wiley & Sons, 2007.
15. ANSYS, Inc., ANSYS Europe, Ltd., Thermal Analysis Guide, ANSYS, Inc., 2025. http://www.ansys.com
16. ANSYS, Inc., ANSYS Europe, Ltd., Structural Analysis Guide, ANSYS, Inc., 2025. http://www.ansys.com
17. Chester, Ashleigh M. et. al. "Loading and thermal behaviour of ZIF-8 metal–organic framework-inorganic glass composites", Dalton Trans., 2024,53, 10655-10665
18. J.F. Wang, J.K. Carson, M.F. North, D.J. Cleland, "A new approach to modelling the effective thermal conductivity of heterogeneous materials," International Journal of Heat and Mass Transfer, 2006, 49 (17–18), 3075–3083. https://doi.org/10.1016/j.ijheatmasstransfer.2006.02.007